The effect of filling density on flammability and mechanical properties of 3D-printed carbon fiber-reinforced nylon

Lucie Zárybnická[1*], Jana Machotová[2], Marek Pagáč[3], Jozef Rychlý[4], Anna Vykydalová[4,5]

[1]Department of Technical Studies, College of Polytechnics Jihlava, Tolstého 16, 586 01 Jihlava, Czech Republic

[2]Institute of Chemistry and Technology of Macromolecular Materials, Faculty of Chemical Technology, University of Pardubice, Studentská 573, 532 10 Pardubice, Czech Republic

[3]Department of Machining, Assembly and Engineering Technology, Faculty of Mechanical Engineering, VSB-TU Ostrava, 17. Listopadu 2172/15, 708 00 Ostrava-Poruba, Czech Republic

[4]Polymer Institute, Slovak Republic, Slovak Academy of Sciences, Dubravská Cesta 9, Bratislava 45, 845 41

[5]Institute of Physical Chemistry and Chemical Physics, Faculty of Chemical and Food Technology, Slovak University of Technology, Radlinského 9, 812 37 Bratislava, Slovakia

*__Corresponding author__: Lucie Zárybnická (E-mail: Lucie.Zarybnicka@vspj.cz)

Abstract

3D printing of reinforced polymeric materials, which provides products of excellent physical and mechanical properties, is at the forefront of interest in the field of additive technologies. To ensure material, time, and financial savings, 3D objects having reduced filling density are frequently prepared. The presented work aims to study the effect of different levels of filling density (18, 42, and 62 % using a honeycomb filling pattern) in contrast to 100 % solid fill of carbon fiber-reinforced polyamide 6.6 materials processed by Fused Filament Fabrication on their flammability and mechanical properties. Concurrently, the effect of a commercial flame retardant additive concerning the filling density was also evaluated. The flammability and mechanical properties of the 3D printed materials were evaluated according to cone calorimeter measurements, and tensile and bending tests, respectively. It was found that the reduction in the filling density led to a pronounced decrease in mechanical properties (of about 40–50 % for tensile and bending stress) and also to the deterioration of flame resistance (of about 50–70 % shorter burning time), with no unambiguous correlation with the respective filling density level used. If significant economic savings are preferred, 3D objects designed with low levels of filling density (18 or 42 %) are advantageous to be manufactured from nylon stabilized with a flame retardant additive, resulting in acceptable fire-resistant properties.

Keywords: 3D printing; Filling density; Nylon; Flame Retardant; Carbon fiber; Cone Calorimeter.

1. Introduction

Additive manufacturing (AM) is a very productive technology that makes products from 3D model data by slicing the 3D shape of an object in flat thin layers of constant thickness, which can be placed one up onto the other [1]. 3D printing was first described in 1986 by Charles Hull (Stereolithography, SLA) [2]. AM is a good method for the cost-effective making of prototyping models of diverse geometrical shapes. Undoubtedly, the most widespread AM technology is Fused Filament Fabrication (FFF) technology, widely used by “do-it-yourselfers” and in industry. Its advantage is the ability to process a large number of different polymer-based materials in the form of filaments. Various types of thermoplastics are most commonly processed, e.g. polylactic acid (PLA) [3–7], polyethylene terephthalate [8], polyethylene terephthalate glycol (PET-G) [9], polystyrene [10,11], polyamide [12,13], polyether ether ketone [14–17], acrylonitrile-butadiene-styrene [18].

Nylon (polyamide 6.6, PA6.6) is one of the most widely used structural thermoplastics processed using AM technologies [19–23]. This material offers a balanced combination of beneficial properties, such as impact resistance, high toughness (even at low temperatures), damping properties, high mechanical strength [24,25] and favorable chemical resistance [26,27]. The typical performance profile is complemented by good abrasion resistance [28], especially in contact with opposing parts with a rough surface. All these characteristics make PA6.6 a classic and universal material used in applications for harsh environments unless critically tight dimensional tolerances are specified [29–33]. In terms of the mentioned knowledge, nylon was chosen for the research within the presented article.

AM technologies offer the possibility of preparing products with different levels of filling density which are provided using various filling patterns. The most widely used filling patterns include honeycomb structures (hexagonal grids), rectangular grids, triangular grids, and concentric lines [34,35]. The filling density and filling pattern were reported to significantly influence the mechanical and physical-chemical properties of 3D products, e.g., triangular and honeycomb filling patterns usually provide favorable tensile and bending properties [36], but they also positively affect the course of 3D object manufacturing in terms of printing time and final product weight, which ultimately determines its price.

Polymers are usually flammable materials and may contribute to the occurrence and spread of fire. Therefore, it is often necessary to systematically address the fire safety of these materials during their use and to take effective preventive measures. For this purpose, flame retardant additives are ordinarily applied to polymers to slow down the pertinent combustion process.

Currently, the development of flame retardant polymers for 3D printing purposes has become a priority for the further expansion of AM technologies [37]. Guo et al. [38] fabricated flame retardant PLA by 3D printing. The authors used the combination of melamine polyphosphate (17 wt. %) and Cloisite 30B (1 wt. %) as flame retardants and a significant decrease in peak heat release rate (around 60 %) was observed in cone calorimeter tests, compared with the neat 3D printed samples. Geoffroy et al. [39] applied aluminum tri-hydroxide and expandable graphite as flame retardant additives for 3D-printed ethylene-vinyl acetate (EVA) polymer. They found that the incorporation of 65 wt. % of aluminum tri-hydroxide decreased the peak heat release rate (pHRR) and total heat release (THR) by 80 and 50 %, respectively, and increased the time to ignition (TTI) by 70 %, compared with neat EVA. Kolibaba et al. [40] used a polyelectrolyte complex, composed of polyvinylamine and sodium polyphosphate, as a flame retardant additive for 3D-printed PLA. A significant reduction in the pHRR (40 %) and THR (20 %) was observed in the material containing 25 wt. % of the flame retardant compared with the neat PLA printed sample. Koo et al. [41] reported the preparation of flame retardant polyamide 6 for 3D printing purposes which contained a mixture of organic aluminum phosphinate (15 wt. %), Cloisite 30B (5 wt. %), and a maleated triblock copolymer containing styrene-hydrogenated butadiene-styrene (5 wt. %). The results confirmed the enhanced flame retardancy of 3D-printed samples.

However, the level of filling density along with the designed filling pattern can significantly influence the fire resistance of a 3D polymeric product, although this phenomenon has been reported only sparingly in the relevant literature [37]. In a study [42] dealing with 3D-printed PLA without the addition of flame retardants, different filling densities were tested. It was observed that decreasing the filling density decreased fuel load and time to ignition. Geoffroy et al. [43] studied the behavior of EVA comprising a flame retardant proving that it is possible to achieve material savings with regard to maintaining good flammability parameters in the case of applying the sandwich filling pattern. Also, the study by Zarybnicka et al. [44] dealt with the combined effect of a flame retardant additive and the structure of products made from PET-G using FFF with different filling patterns finding that decreasing the filling density led to a lower heat release rate and suppressed smoke evolution during combustion.

Appropriately selected reinforcing fibers provide the polymer composites with better mechanical and physical properties [45]. In terms of applications, carbon fibers are among the most widespread reinforcing fibers that show progressive deformation behavior (i.e., the value of tensile modulus increases with increasing load), high strength and tensile modulus values up to 500 °C, low density, extremely high corrosion resistance (not only resistant to the strong oxidizing environment), high resistance to long-term dynamic stress. Moreover, the burning rate of a polymer composite containing carbon fibers is very low [42,46,47].

The presented work deals with preparing 3D-printed carbon fiber-reinforced nylon composites printed in a honeycomb filling pattern, differing in the level of filling density, and the presence (absence) of a commercial flame retardant additive. The materials were tested from the point of view of mechanical properties and especially the combustion behavior. Instead of changing the formulation of starting materials, the optimization of filling density was investigated to ensure favorable performance together with material and time savings.

2. Experimental part

2.1 Materials

Two types of PA6.6 filaments have been tested: a commercial micro carbon fiber-reinforced nylon filament Onyx (marked F_REF) without a flame retardant additive and a flame-resistant variant Onyx FR (marked F_FR) with a combination of a flame retardant (a non-halogenated type, the exact composition is kept secret by the manufacturer) and micro carbon fiber reinforcement. These filaments were manufactured by Markforged (Markforged Inc., USA).

2.2 Preparation of 3D-printed samples

3D printer Markforged X7 (Markforged Inc., USA) processing materials by FFF was used. The 3D-printed samples were prepared according to the same principle for all tests, with filling densities of 18, 42 and 62 % provided by a hexagonal (honeycomb) filling pattern and a filling density of 100 % (using a solid filling pattern). The choice of the particular filling density values was based on the maximum limit value of 62 % for a honeycomb filling pattern recommended by SW Eiger (Markforged Inc., USA).

Fig. 1 shows the design of 3D-printed samples. Three sets of samples with different infills (interior structures) in the honeycomb filling pattern were created. The number of roof and floor layers and the number of perimeters (number of walls) were the same for all samples, namely 4 floor layers, 4 roof layers and 2 walls were always printed in the case of all samples.

The 3D-printed samples were labelled as **X_y**, where **X** represents the filament type (REF or FR), **y** is a percentage of filling density. Based on the recommended parameters of the filament supplier, nozzle temperatures of 275 and 250 °C for Onyx and Onyx FR filaments, respectively, were used. In both cases, a brass nozzle with a diameter of 0.4 mm was used. The printing was performed on an unheated bed made of ground composite. The parameters for 3D-printed sample types are given in Tables S1–S4.

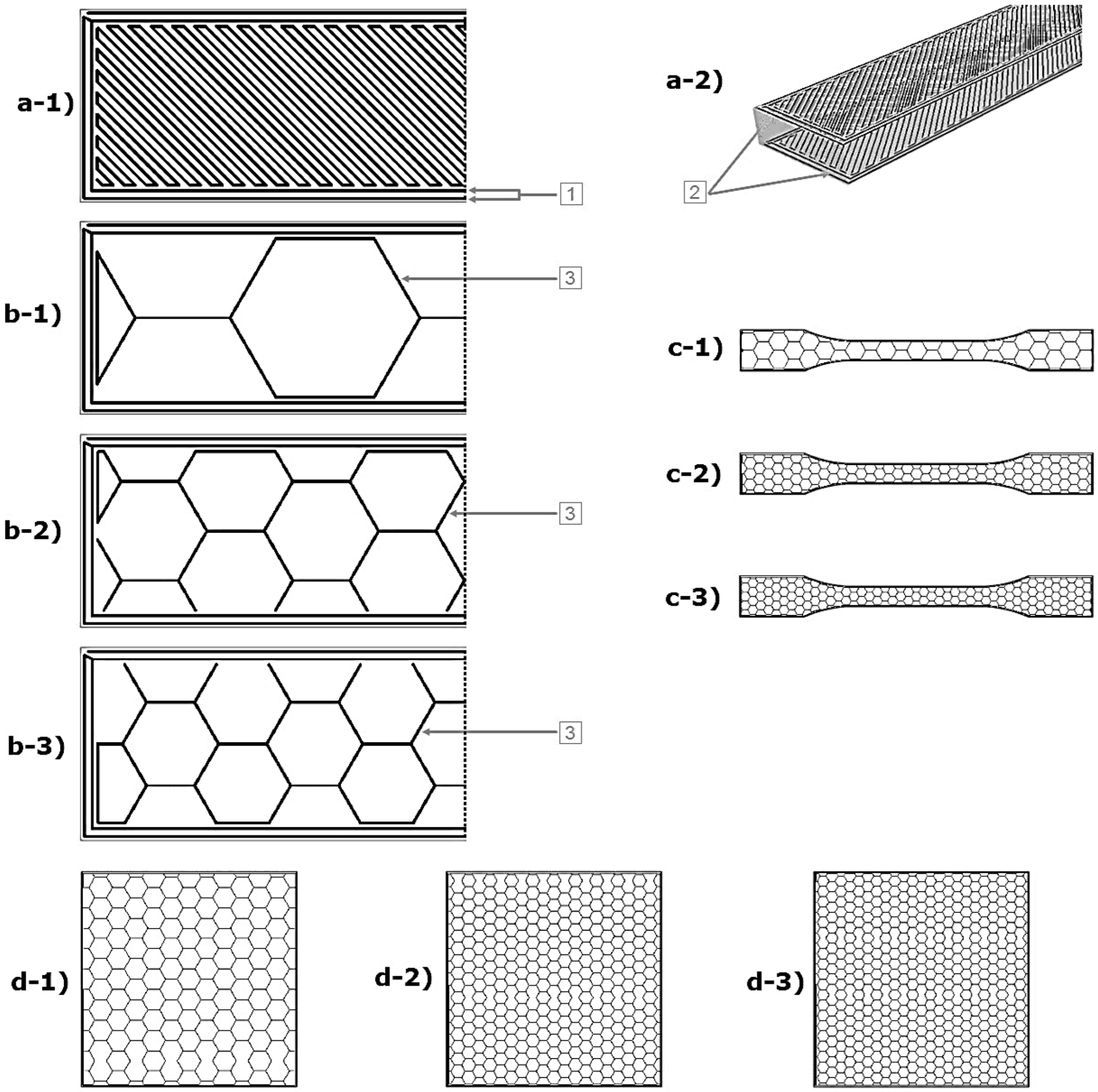

Fig. 1 Representation of samples, trajectories, roof, floor and infills (shown without scale, for illustration only): a-1) cut of the 1st to 4th (17th to 20th) layers of samples for bending testing, 1 - wall layers (two walls); a-2) isometric view of samples for bending testing, 2 - roof (four layers) and floor (four layers); b) samples (infills) for bending testing with filling densities of 18 % (b-1), 42 % (b-2) and 62 % (b-3), 3 - filling trajectory, c) samples (infills) for tensile testing with filling densities of 18 % (c-1), 42 % (c-2) and 62 % (c-3), d) samples (infills) for cone calorimeter measurements with filling densities of 18 % (d-1), 42 % (d-2) and 62 % (d-3).

2.3 Methods

The thermo-physical behaviour (i.e., weight loss and melting temperature (T_m)) of starting filaments was evaluated by performing simultaneous thermogravimetry (TGA) with differential thermal analysis (DTA) under non-isothermal conditions with a STA504 instrument (BÄHR-Thermoanalyse, Germany). Measurements were performed in a nitrogen atmosphere at a heating rate of 20 °C.min^{-1}, in the temperature range of 30–700 °C. Filaments were cut into small rectangular pieces weighing approximately 10–20 mg.

Images of the starting filaments and the printed samples were taken using a Keyence VHX-6000 optical microscope (Keyence, USA) with VHX-S600E free-angle observation system (Z-motorized). Filament samples were observed as cross-sections, where the samples were fixed in commercial resin and then polished using a Qpol (Saphir) 250 M1 Single Disc Manual Grinder/ Polisher (ATM GmbH, DE). The printed samples were also characterized in terms of the surface quality and surface roughness which were calculated by the software.

Glass transition temperature (T_g) and T_m of the printed samples were determined by thermal-mechanical analysis (TMA) using a TMA CX04R instrument (R.M.I. Pardubice, Czech Republic). Sample dimensions were 5×5×5 mm^3, an inserted force was 50 mN, measurements were performed in an air atmosphere under the following conditions: 1) cooling to –20 °C at a rate of 3 °C.min^{-1}, 2) heating to 160 °C at a rate of 3 °C.min^{-1}, 3) cooling to –20 °C at a rate of 3 °C.min^{-1}, 4) heating to 160 °C at a rate of 3 °C.min^{-1}. To determine the T_m, a sample was heated to 300 °C at a rate of 3 °C.min^{-1}.

A universal mechanical device (Instron 3345, USA) with a load of 5 kN was used to test the tensile properties. The tensile test was undertaken at a speed of 1 mm.min^{-1} with a load of 5 kN. The test was performed according to ISO 527-1 [48]. Samples for the tensile test were prepared as dog bones with dimensions according to CSN EN ISO 527-2 [48]. The same instrument performed the bending test with a speed of 1 $mm.min^{-1}$ and a load of 5kN. Dimensions of samples for the bending test were 80×10×4 mm^3.

The flammability of the 3D-printed samples was analysed using cone calorimeter measurements performed with a Fire Testing Technology cone calorimeter (West Sussex, UK), according to the ISO 5660-1 [49] standard under an external heat flux of 50 $kW.m^{-2}$. The dimensions of the samples were 94×94×5 mm^3. The main characteristics measured in this test were: the mean heat release rate (HRR) ($kW.m^{-2}$), the time to ignition TTI (s), the total oxygen consumption (TOC) ($g.g^{-1}$), the total smoke release (TSR) ($m^2.m^{-2}$), the maximum average rate of heat emission (MARHE) ($kW.m^{-2}$), and the total heat release (THR) ($kJ.m^{-2}$). The mean heat release rate (HRR) values were obtained during the time interval 0–489 s. All samples were measured three times to confirm the reproducibility within ± 5 %.

3. Results and discussion

3.1 Characterization of filament materials

Knowledge of the thermo-physical properties of a polymer filament is very important for setting the correct 3D printing parameters (especially bed and nozzle temperatures) [50]. Both polymer filament materials were characterized in terms of T_m and the content of non-degradable components using DTA-TGA (Fig.2), performed under a nitrogen atmosphere. The results of T_m, obtained from DTA thermograms, correlate with the literature [51]. F_REF exhibited T_m of 194.3 °C and contained approximately 10 wt.% of non-degradable residue composed predominantly of carbon fibers [52], while the F_FR, having almost the same T_m (195.0 °C), contained approximately 17 wt.% of the non-degradable components. The difference between the content of non-degradable residues can be attributed to the presence of the flame retardant additive. It can also be seen from the DTA curves in the region around 100 °C that both types of polymer filaments contained a low amount of absorbed moisture [52]. Under the inert atmosphere, the F_FR showed an earlier onset of thermal degradation (403.0 °C) compared to the F_REF (438.3 °C). It can be concluded that the presence of the flame retardant additive does not significantly affect the thermo-physical properties of the carbon fiber-reinforced nylon filament in the range of considered 3D printing temperatures [53,54].

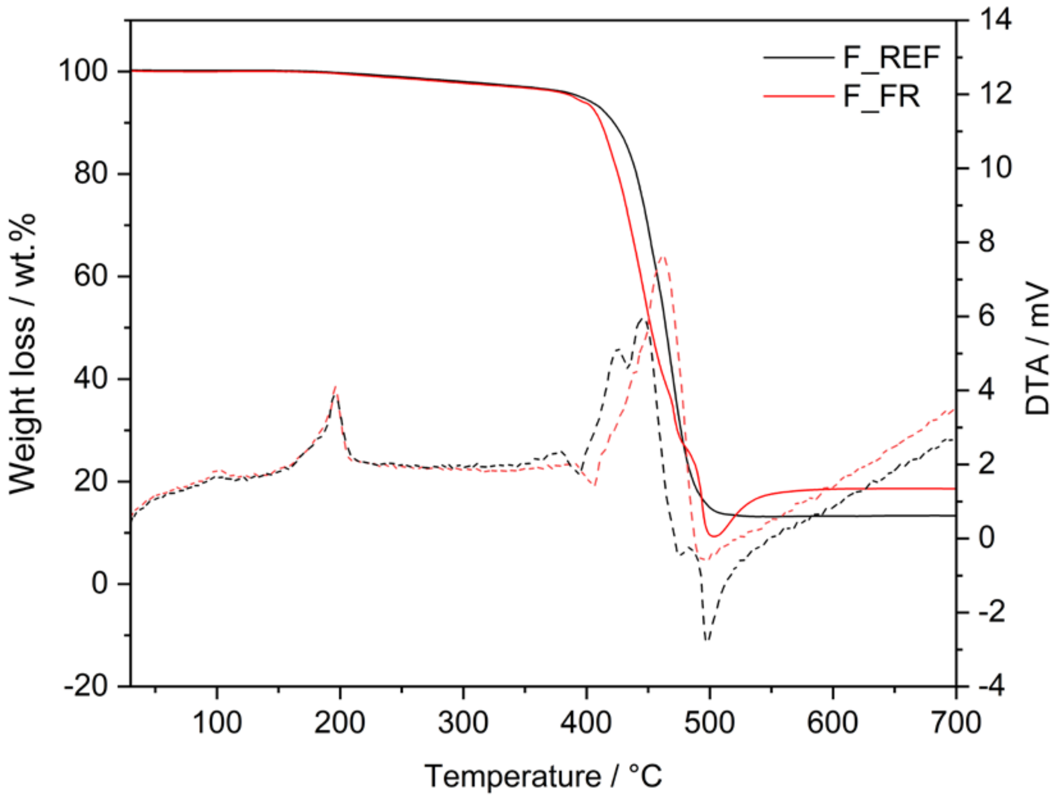

Fig. 2 TGA (solid lines) and DTA (dashed lines) thermograms for F_REF (black lines) and F_FR (red lines).

The presence and distribution of carbon fibers and flame retardant additive particles were monitored on cross-sections of filaments (Figure 3). The ends of the carbon fibers are marked with a red arrow, and the flame retardant additive is pointed with a blue arrow. In both cases, the reinforcing carbon fibers were homogeneously distributed in the polymer matrix. For the F_FR filament, flame retardant particles were also clearly observed.

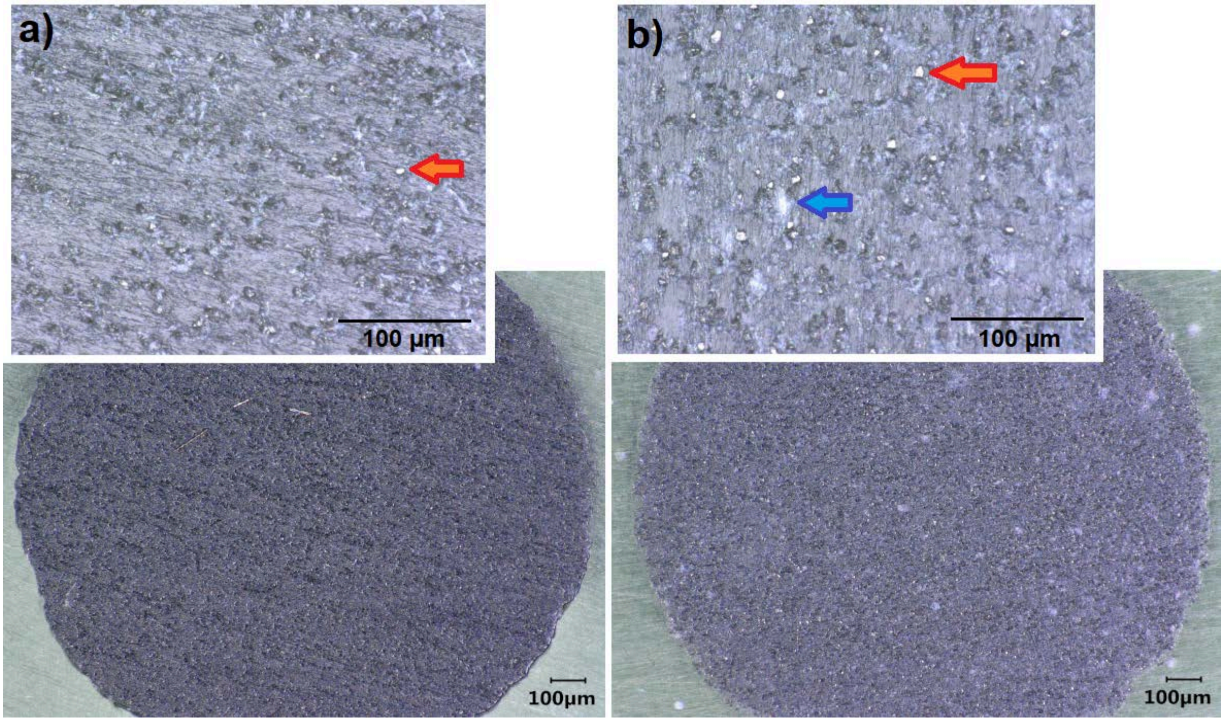

Fig. 3 Images of cross-sections of both types of filaments: a) F_REF, b) F_FR.

3.2 Testing of 3D-printed samples

The prepared samples were characterized from the point of view of T_g and T_m, which are important characteristics that can determine useful properties and industrial applications. The 3D-printed materials having a 100 % solid fill were tested by TMA, performed under an air atmosphere, where the coefficients of thermal expansion α_1 (in the glassy region) and α_2 (in the rubbery region) were also determined. T_g values of 56.4 and 54.9 °C were determined for the samples REF_100 and FR_100, respectively. It is evident that the presence of the flame retardant additive didn´t affect T_g significantly. Regarding the results of α_1 in the glassy region, the values of 63.26 and 24.1 ppm /°C were determined for the samples REF_100 and FR_100, respectively. In the rubbery region, the α_2 values of 305.33 and 115.41 ppm /°C were found for the samples REF_100 and FR_100, respectively. These results reveal that the FR_100 shows lower expansion, which may have a positive effect on the dimensional stability of the product during the 3D printing process and in industrial applications involving thermal load. T_m values of 187.8 and 206.3 °C were determined for the samples REF_100 and FR_100, respectively. It is evident that the values obtained using TMA differ from the values from TGA-DTA. The following factors may be responsible for this difference: (i) samples were mechanically stressed during TMA analysis, (ii) different temperature programs were used in both analyses, (iii) last but not least, the samples underwent additional temperature stress during 3D printing. Therefore, the thermal history of processing can be reflected in the results.

From its theoretical basis, the FFF technology can prepare smooth samples whose surface roughness is affected by 3D printing parameters, such as the minimum layer, the temperature of the pad, and the temperature and thickness of the nozzle [55]. In the case of reinforced filaments, the surface roughness of 3D-printed objects is always affected by a reinforcing additive incorporated in the polymer matrix, reflecting its shape, amount, and size [56]. The surface of the roof (top layer) of 3D-printed samples was evaluated using a digital optical microscope to monitor the overall quality (Fig. 4) and the surface roughness (Table 1). It can be seen that the roof surface of samples containing a combination of a flame retardant additive and carbon fibers (FR) appears more compact and smoother compared to samples added only with carbon fibers (REF), which is in good accordance with the results of lower thermal expansion coefficients in case of the FR material. The filling density was shown to affect the roof surface quality as well; the increased the filling density of the honeycomb structure, the higher the surface roughness of the roof. On the contrary, the samples with 100 % solid fill appeared to have the best quality of the roof surface, probably because the decrease in the number of air pockets in the infill structure resulted in a smaller amount of roof surface deformation. The results of optical microscopy suggest that the testing of mechanical properties and fire resistance should not be affected significantly by roof surface quality.

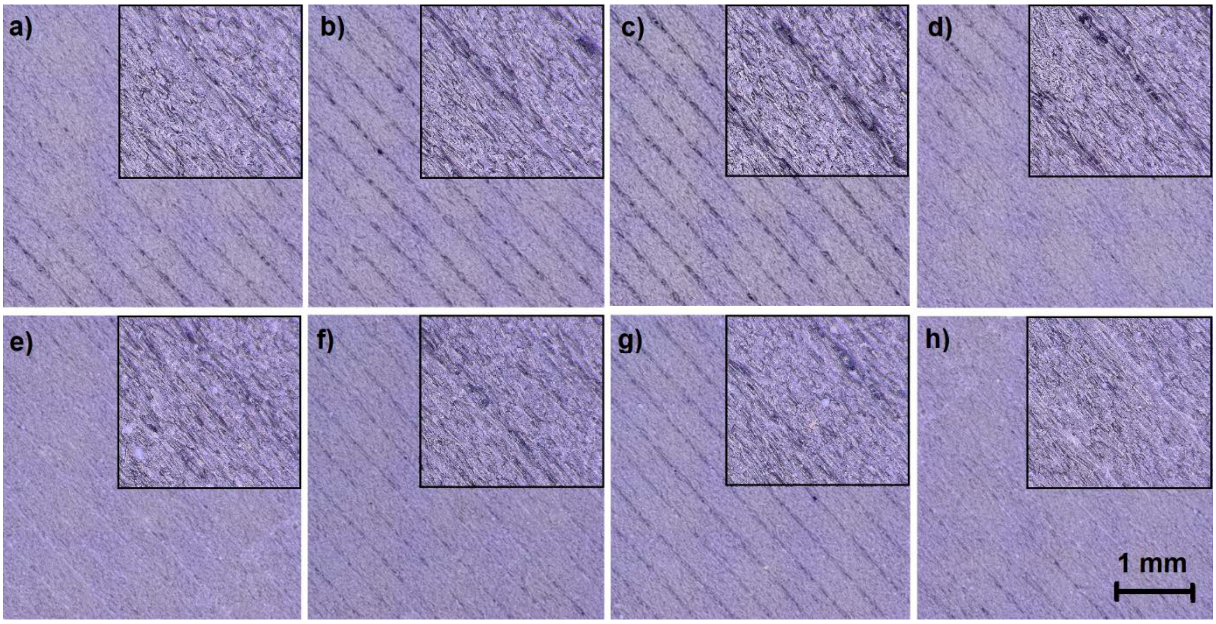

Fig. 4 Microscopy pictures of the roof surface for all the prepared samples: a) REF_18, b) REF_42, c) REF_62, d) REF_100, e) FR_18, f) FR_42, g) FR_62, h) FR_100.

Table 1 Results of surface roughness measurement.

Sample	S_a^* / µm	S_z^* / µm
REF_18	13.3±0.01	131.0±1.1
REF_42	13.0±0.02	123.8±0.9
REF_62	15.6±0.02	135.5± 0.8
REF_100	11.2±0.01	101.7±0.6
FR_18	11.7±0.02	123.0±1.1
FR_42	15.6±0.03	144.3±1.1
FR_62	16.5±0.03	134.2±1.0
FR_100	12.9±0.02	151.8±1.2

*S_a and S_z parameters are the extensions of R_a (arithmetical mean height of a line) and R_z (difference between the tallest and deepest peaks on the surface), respectively.

The 3D-printed samples differing in filling density were subjected to mechanical testing. The tensile and bending properties are the basic characteristics important for industrial applications. Tensile tests (Table 2) revealed that as the filling density increased from 18 to 62 %, Young´s modulus and tensile stress slightly increased, while the elongation at break wasn´t affected significantly. On the contrary, bending tests (Table 2) showed that Young's modulus decreased sparingly increasing the filling density, while the bending stress and elongation at the break didn’t change pronouncedly. Comparing REF and FR samples with 18, 42 and 62 % of filling density, the FR samples exhibited lower tensile stress because the flame retardant additives could act as stress concentration points, thereby reducing the strength. Other results were comparable within the measurement error.

Focusing on the 100 % solid fill samples, the tensile test results showed higher values in all aspects compared to the samples prepared with decreased filling densities. This phenomenon reflects material discontinuity in the case of applying the honeycomb filling pattern. As expected, the REF_100 material also performed better than FR_100 in all respects due to the absence of another kind of inhomogeneity in the form of the flame retardant additive [57]. Looking at the bending test results, the REF_100 and FR_100 samples showed higher bending stress values compared with the samples of lower filling densities, where the same trend can be seen in the case of tensile stress. Generally, a higher carbon fiber content material shows better tensile and bending performance [58].

In contrast, Young's modulus and elongation results of bending testing were found to be higher for the samples with lower filling densities. This effect can be related to the higher stiffness of full samples, which provided lower or comparable flexibility. It can be concluded that lowering the level of filling density of 3D-printed carbon fiber-reinforced nylon samples with a honeycomb filling pattern decreased the tensile performance of printed samples but showed a minor effect on bending properties.

Table 2 Results of mechanical testing - tensile and bending tests.

Sample	Tensile test			Bending test		
	Young's modulus / MPa	Elongation at maximum load / %	Tensile stress / MPa	Young's modulus / MPa	Elongation at maximum load/ mm	Bending stress / MPa
REF_18	311.54 ± 7.58	16.78 ± 0.22	18.75 ± 0.55	602.22 ± 17.74	8.13 ± 0.29	21.26 ± 0.55
REF_42	325.93 ± 8.79	16.95 ± 0.31	18.57 ± 0.22	464.29 ± 22.15	9.90 ± 0.25	19.28 ± 0.65
REF_62	328.94 ± 19.81	17.60 ± 0.22	19.44 ± 0.81	457.14 ± 9.35	10.00 ± 0.24	19.13 ± 0.65
REF_100	1402.7 ± 47.59	20.61 ± 0.87	36.68 ± 0.52	605.65 ± 29.57	8.28 ± 0.09	33.23 ± 1.24
FR_18	442.22 ± 6.67	12.31 ± 0.64	15.55 ± 0.45	729.79 ± 27.49	9.73 ± 0.35	21.92 ± 0.49
FR_42	454.11 ± 4.44	11.79 ± 0.08	15.55 ± 0.15	603.66 ± 26.49	9.27 ± 0.30	21.24 ± 0.68
FR_62	509.34 ± 15.67	11.80 ± 0.50	17.15 ± 0.72	578.36 ± 20.81	9.67 ± 0.23	21.52 ± 0.88
FR_100	1241.55 ± 99.53	18.30 ± 0.69	25.75 ± 1.29	662.47 ± 24.54	7.67 ± 0.13	30.82 ± 1.39

3.3 Flammability of 3D-printed samples

The flammability of the prepared samples was tested using cone calorimetry, being recognized as the best tool for analyzing the fire behavior of polymers [59]. The results of the most important parameters can be seen in Table 3. Focusing on the burning time, it was found that the FR samples exhibited a longer burning time compared to the corresponding REF samples, which confirms the effectiveness of the non-halogenated flame retardant used. In general, non-halogenated flame retardants show the action by forming an insulating protective layer in the condensed phase or releasing inflammable compounds to dilute oxygen in the gaseous phase [60]. With regard to the effect of the filling density, it was found that burning time decreased with reducing the filling density. This phenomenon is probably associated with sample weight and the cell size in the honeycomb structure of the 3D-printed samples. The higher the sample weight (i.e., the polymer content in the sample), the longer burning. As for the effect of the cell size (i.e., the volume of air pockets in the sample) that is directly related to the respective filling density (see Figure 7 and Table 4), the more air was trapped in a sample, the faster the sample burned since air is a combustion accelerator. In addition, the cell size determines gas and pressure build up in the cells during combustion and may be responsible for the degradation rate. Focusing on TTI, no conclusive relation between the filling density and

TTI was found for both series of samples. Only the sample FR_100 deviated with TTI three times longer than the other samples. ~~In a study [61] where they tested a triangle-type structure, it was observed that increasing the density of the filling density had no effect on the flammability rating parts of constant shell thickness.~~

The other flammability characteristics in terms of the mean HRR, MARHE and THR were shown to be significantly impaired in the case of the samples of both series printed in the honeycomb filling pattern in comparison to the corresponding 100 % solid fill samples, while the effect of the extent of the filling density reduction on the parameters mentioned above was shown to be minimal. Regarding the flame retardant additive presence, it was confirmed that the FR samples were more fire-resistant in terms of HRR, MARHE and THR parameters in contrast to the corresponding REF samples. Focusing on the TSR parameter, a higher smoke evolution was observed for the FR samples, which is apparently a consequence of the dilution effect (by releasing inflammable compounds) caused by the non-halogenated flame retardant used [62]. It was shown that reducing the filling density mitigated the release of smoke during burning, which was manifested especially in the case of the FR series of samples and may represent a favorable phenomenon in terms of the impacts of the fire event on human health and safety.

Sample	Weight loss / wt.%	TTI* / Burning time / s	mean HRR / $kW.m^{-2}.g^{-1}$	TOC / $g.g^{-1}$	TSR / $m^2.m^{-2}.g^{-1}$	MARHE / $kW.m^{-2}.g^{-1}$	THR / $MJ.m^{-2}.g^{-1}$
REF_18	85.96 ± 0.1	29 / 293 ± 4	13.9 ± 0.48	37.8 ± 1.2	16.45 ± 0.27	15.49 ± 0.60	3.61 ± 0.14
REF_42	84.40 ± 0.6	35 / 339 ± 9	11.58 ± 0.21	40.9 ± 0.3	15.10 ± 1.65	13.54 ± 0.50	3.49 ± 0.03
REF_62	83.75 ± 0.7	39 / 353 ± 29	11.68 ± 0.71	39.9 ± 0.9	17.82 ± 2.91	13.51 ± 0.70	3.51 ± 0.07
REF_100	87.99 ± 0.3	41 / 746 ± 93	5.99 ± 0.14	84.8 ± 5.4	16.93 ± 2.45	5.80 ± 0.60	3.85 ± 0.26
FR_18	81.02 ± 1.7	29 / 469 ± 28	7.81 ± 0.77	36.6 ± 6.4	41.46 ± 0.84	10.20 ± 0.54	3.46 ± 0.57
FR_42	78.78 ± 2.2	34 / 497 ± 6	6.81 ± 0.10	32.8 ± 0.0	45.40 ± 2.08	8.93 ± 0.29	3.17 ± 0.02
FR_62	77.50 ± 1.7	31 / 457 ± 18	7.49 ± 0.16	36.6 ± 1.2	48.63 ± 1.14	9.42 ± 0.17	3.19 ± 0.06

FR_100	76.37 ± 2.6	90 / 1742 ± 104	1.66 ± 0.02	60.2 ± 4.9	71.36 ± 3.69	1.82 ± 0.11	2.72 ± 0.22

Table 3 Flammability results.

*Standard deviation ranged between 1−2 s for every sample.

The course of HRR and TSR over time can be seen in Fig. 5. In the case of the FR samples. The HRR curves exhibited two distinct peaks and a plateau. The first peak, associated with sample ignition and development of fire, was more pronounced. As the HRR is proportional to the oxygen consumed, this means that a large amount of oxygen was consumed in the early stages of burning. The second peak, demonstrating a fully developed fire, appeared after approximately 200 second of burning when the fire and heat penetrated the sample. This peak is highly attributed to the degradation and damages of a char layer under heat flux.

On the contrary, the shape of the HRR curves of the REF samples resembled one broad peak without a plateau, suggesting a uniform combustion process. When considering the HRR curves´ character, the FR samples can behave as thermally thick charring (residue forming) materials showing an initial increase in HRR until an efficient char layer is formed. In contrast, the REF samples showed curves typical for intermediate non-charring materials [63].

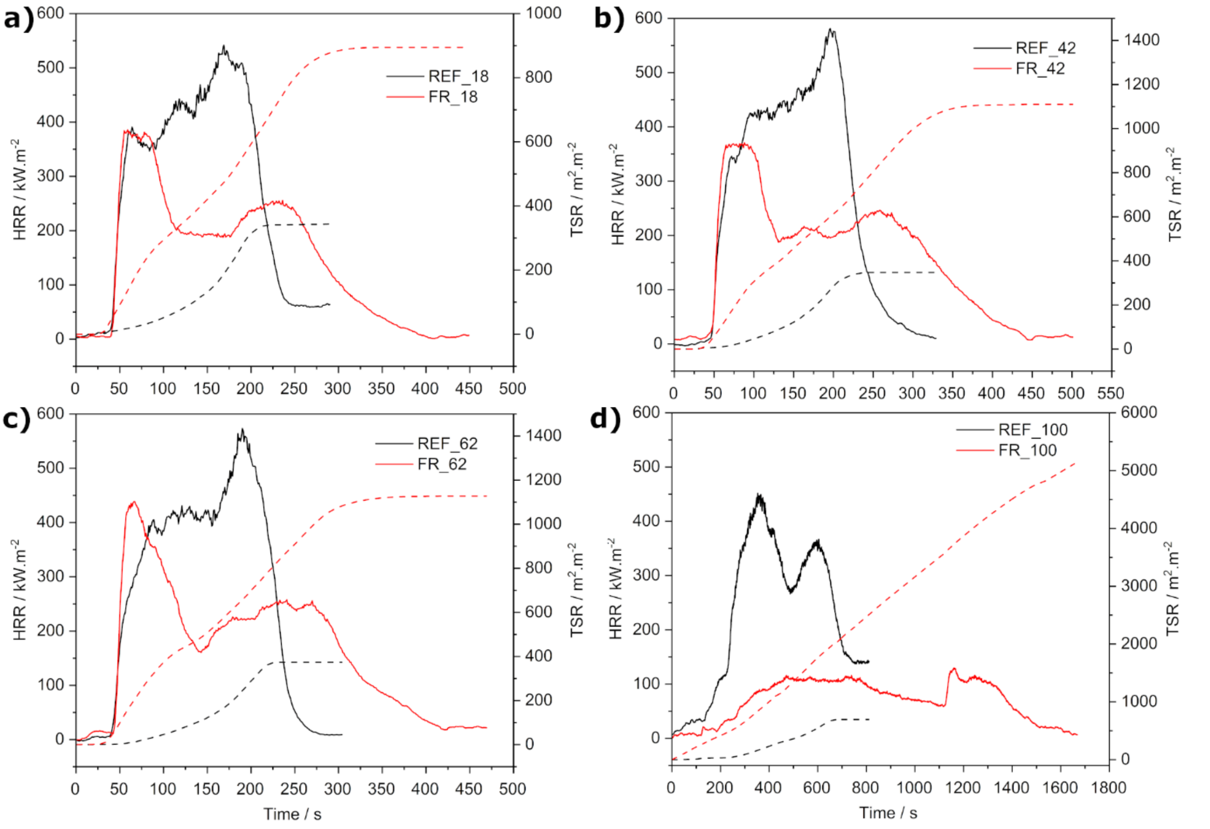

Fig. 5 Graphic dependences of HRR (solid lines) and TSR (dashed lines) on burning time for 3D-printed samples with different filling densities: a) 18 %, b) 42 %, c) 62 %, d) 100 % solid fill.

For an illustration of the effect of combustion on the appearance of burnt samples, the images of the 3D-printed samples were taken before and after the burning test (see Figure 6). REF samples charred forming porous and rough residues, while the charred residues of the FR samples were smoother and more compact except for the FR_100 sample, the residue of which was “swollen”, which indicates a huge amount of smoke released during combustion. The filling density was shown to affect the character of the charred residue as well, the lower the filling density, the rougher the charred residue. This phenomenon could be attributed to the cell size given by the respective filling density. The higher the cell size, the stronger the pressure build up in the cells during burning, which may result in a heavy char layer damage.

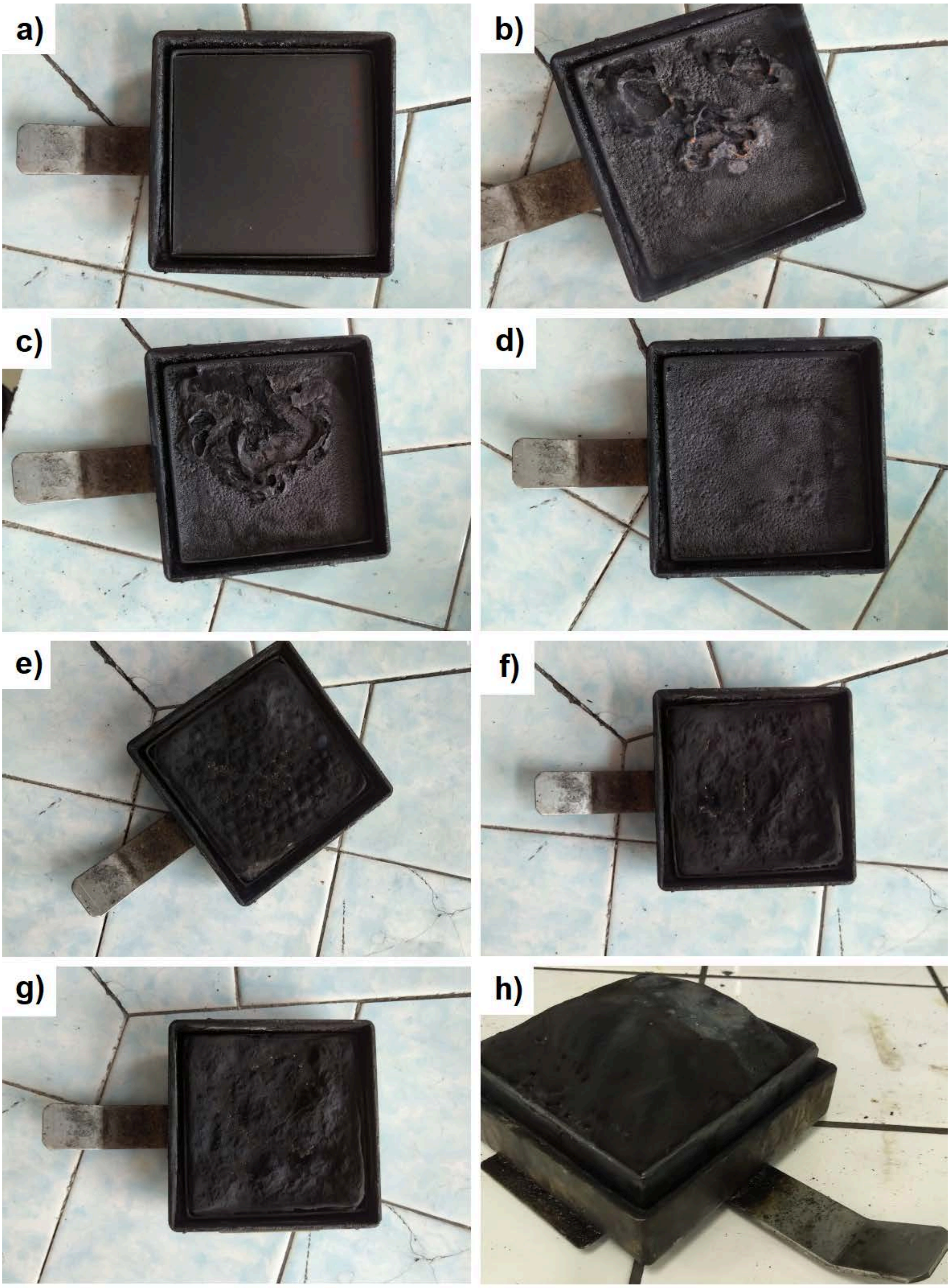
a)
b)
c)
d)
e)
f)
g)
h)

Fig. 6 Samples before and after the cone calorimeter test: a) REF_18 before, b) REF_18 after, c) REF_42 after, d) REF_62 after, e) FR_18 after, f) FR_42 after, g) FR_62 after, h) FR_100 after.

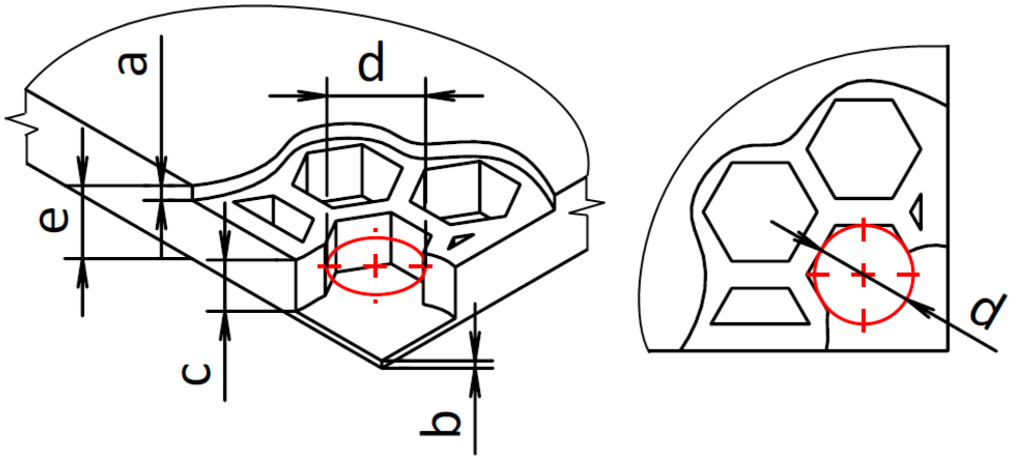

Fig. 7 Cell parameters: a) roof layer, b) floor layer, c) cell height, d) diameter of the inscribed circle of the cell, e) sample height; (graphical representation only).

Table 4 Cell volume (cell size) in honeycomb structures for different filling densities.

Parameters	Filling density / %		
	18	42	62
Diameter of the inscribed circle of the cell / mm	7.9	4.6	3.8
Cell height = sample height – roof layers – floor layers / mm	5 – 4 × 0.125 – 4 × 0.125 = 4		
Cell size / mm^3	216.19	73.30	50.02

3.4 Financial and time savings of the 3D printing process

An important parameter of industrial products manufactured with AM technology is saving money and time, which can be tuned significantly by lowering the level of filling density. Although the information reflecting this issue can be found in Tables S1–S4, where, however, the effect of the filling density reduction on time, material and financial savings is not very convincing due to the small dimensions of samples. Economic savings become more pronounced, especially for larger objects, which is demonstrated in Table 5, describing a design of a model carbon fiber-reinforced PA6.6 sample with dimensions of 100 × 100 × 100 mm^3.

This example shows that significant savings can be achieved even at the filling density of 62 % provided in a honeycomb filling pattern.

Table 5. 3D printing parameters of a model large-size carbon fiber-reinforced nylon sample.

Parameters				
Dimensions:	100 mm × 100 mm × 100 mm			
Layer Height:	0.2 mm			
Number of Layers:	500			
Filling Pattern:	Hexagonal Fill (Honeycomb)			Solid Fill
Filling Density:	**18 %**	**42 %**	**62 %**	**100 %**
Print Time:	15 h 59 min	1 d 0 h	1 d 4 h	2 d 9 h
Final Part Mass:	209.34 g	301.62 g	337.16 g	1 140 g
Roof and Floor layers:	4			
Wall Layers:	2			
Plastic Angles:	90° (not set at one angle)			
Material Cost per 1 pcs:	REF 42.13 USD/ FR 51.00 USD	REF 60.71 USD/ FR 73.49 USD	REF 67.86 USD/ FR 82.15 USD	REF 229.77 USD/ FR 278.14 USD

Conclusion

The presented article deals with the influence of filling density (18, 42, 62 %, printed in a honeycomb structure filling pattern, and 100 % solid fill) on flammability and mechanical properties of carbon fiber-reinforced nylon products processed by FFF AM technology. The optimization of filling density was studied to ensure favorable fire behavior and mechanical performance together with the material, financial and time savings. It was demonstrated that significant savings in the 3D printing process could be obtained by reducing the filling density at the expense of a pronounced decrease in mechanical properties (40–50 % for tensile and bending stress) and the deterioration of flame resistance (50–70 % in terms of burning time shortening) of 3D nylon objects. Nevertheless, no conclusive correlation between the specific level of reduced filling density and the properties of 3D products was proved. If economic savings together with favorable fire-resistant properties are required, it is convenient to produce 3D objects of low filling density made of nylon stabilized with a flame retardant additive.

Acknowledgment

This study was conducted in association with the project Innovative and Additive Manufacturing Technology−New Technological Solutions for 3D Printing of Metals and Composite Materials (reg. no. CZ.02.1.01/0.0/0.0/17_049/0008407) financed by Structural Funds of the European Union and by the project Students Grant Competition SP2022/50 financed by the Ministry of Education, Youth and Sports and Faculty of Mechanical Engineering, VSB−Technical University of Ostrava.

References

[1] C. Gosselin, R. Duballet, P. Roux, N. Gaudillière, J. Dirrenberger, P. Morel, Large-scale 3D printing of ultra-high performance concrete–a new processing route for architects and builders, Mater. Des. 100 (2016) 102–109.

[2] M. Pagac, J. Hajnys, Q.-P. Ma, L. Jancar, J. Jansa, P. Stefek, J. Mesicek, A Review of Vat Photopolymerization Technology: Materials, Applications, Challenges, and Future Trends of 3D Printing, Polymers (Basel). 13 (2021) 598.

[3] R. Baptista, M. Guedes, Morphological and mechanical characterization of 3D printed PLA scaffolds with controlled porosity for trabecular bone tissue replacement, Mater. Sci. Eng. C. 118 (2021) 111528.

[4] A. Yonezawa, A. Yamada, Deterioration of the Mechanical Properties of FFF 3D-Printed PLA Structures, Inventions. 6 (2021) 1.

[5] S.R. Rajpurohit, H.K. Dave, Impact strength of 3D printed PLA using open source FFF-based 3D printer, Prog. Addit. Manuf. 6 (2021) 119–131.

[6] F. Lavecchia, M.G. Guerra, L.M. Galantucci, Chemical vapor treatment to improve surface finish of 3D printed polylactic acid (PLA) parts realized by fused filament

fabrication, Prog. Addit. Manuf. (2021) 1–11.

[7] R. Torre, S. Brischetto, I.R. Dipietro, Buckling developed in 3D printed PLA cuboidal samples under compression: Analytical, numerical and experimental investigations, Addit. Manuf. 38 (2021) 101790.

[8] F.A. Doronin, Y. V Rudyak, G.O. Rytikov, A.G. Evdokimov, V.G. Nazarov, 3D-printed planar microfluidic device on oxyfluorinated PET-substrate, Polym. Test. 99 (2021) 107209.

[9] K. Sharma, Effect of FFF process parameters on density and mechanical properties of PET-G and carbon fiber reinforced PET-G composites, (2021).

[10] S. Singh, G. Singh, K. Sandhu, C. Prakash, R. Singh, Investigating the optimum parametric setting for MRR of expandable polystyrene machined with 3D printed end mill tool, Mater. Today Proc. 33 (2020) 1513–1517.

[11] M. Sevastaki, M.P. Suchea, G. Kenanakis, 3D Printed Fully Recycled TiO2-Polystyrene Nanocomposite Photocatalysts for Use against Drug Residues, Nanomaterials. 10 (2020) 2144.

[12] M. Utzeri, E. Farotti, M. Coccia, E. Mancini, M. Sasso, High strain rate compression behaviour of 3D printed Carbon-PA, J. Mater. Res. (2021) 1–11.

[13] M. Kubota, K. Hayakawa, A. Todoroki, Effect of build-up orientations and process parameters on the tensile strength of 3D printed short carbon fiber/PA-6 composites, Adv. Compos. Mater. (2021) 1–18.

[14] Y. Wang, W.-D. Müller, A. Rumjahn, F. Schmidt, A.D. Schwitalla, Mechanical properties of fused filament fabricated PEEK for biomedical applications depending on additive manufacturing parameters, J. Mech. Behav. Biomed. Mater. 115 (2021) 104250.

[15] K. Rodzeń, E. Harkin-Jones, M. Wegrzyn, P.K. Sharma, A. Zhigunov, Improvement of the layer-layer adhesion in FFF 3D printed PEEK/carbon fibre composites, Compos. Part

A Appl. Sci. Manuf. 149 (2021) 106532.

[16] A. El Magri, S. Vanaei, S. Vaudreuil, An overview on the influence of process parameters through the characteristic of 3D-printed PEEK and PEI parts, High Perform. Polym. (2021) 09540083211009961.

[17] K. Rodzeń, P.K. Sharma, A. McIlhagger, M. Mokhtari, F. Dave, D. Tormey, R. Sherlock, B.J. Meenan, A. Boyd, The Direct 3D Printing of Functional PEEK/Hydroxyapatite Composites via a Fused Filament Fabrication Approach, Polymers (Basel). 13 (2021) 545.

[18] J.S. Chohan, N. Mittal, R. Kumar, S. Singh, S. Sharma, J. Singh, K.V. Rao, M. Mia, D.Y. Pimenov, S.P. Dwivedi, Mechanical strength enhancement of 3D printed acrylonitrile butadiene styrene polymer components using neural network optimization algorithm, Polymers (Basel). 12 (2020) 2250.

[19] J. Jiang, Z. Li, H. Yang, X. Wang, Q. Li, L.-S. Turng, Microcellular injection molding of polymers: a review of process know-how, emerging technologies, and future directions, Curr. Opin. Chem. Eng. 33 (2021) 100694.

[20] A.C. Corrêa, E. de Morais Teixeira, V.B. Carmona, K.B.R. Teodoro, C. Ribeiro, L.H.C. Mattoso, J.M. Marconcini, Obtaining nanocomposites of polyamide 6 and cellulose whiskers via extrusion and injection molding, Cellulose. 21 (2014) 311–322.

[21] A. Hassan, P.R. Hornsby, M.J. Folkes, Structure–property relationship of injection-molded carbon fibre-reinforced polyamide 6, 6 composites: the effect of compounding routes, Polym. Test. 22 (2003) 185–189.

[22] M. Yuan, L. Turng, S. Gong, D. Caulfield, C. Hunt, R. Spindler, Study of injection molded microcellular polyamide-6 nanocomposites, Polym. Eng. Sci. 44 (2004) 673–686.

[23] P.A. Santos, M.A.S. Spinacé, K.K.G. Fermoselli, M.-A. De Paoli, Polyamide-6/vegetal

fiber composite prepared by extrusion and injection molding, Compos. Part A Appl. Sci. Manuf. 38 (2007) 2404–2411.

[24] T.S. Ghanta, S. Aparna, N. Verma, D. Purnima, Review on nano-and microfiller-based polyamide 6 hybrid composite: Effect on mechanical properties and morphology, Polym. Eng. Sci. 60 (2020) 1717–1759.

[25] J.W. Yoon, Y. Park, J. Kim, C.H. Park, Multi-jet electrospinning of polystyrene/polyamide 6 blend: thermal and mechanical properties, Fash. Text. 4 (2017) 1–12.

[26] S. Asiaban, S. Moradian, Investigation of tensile properties and dyeing behavior of various polypropylene/polyamide 6 blends using a mixture experimental design, Dye. Pigment. 92 (2012) 642–653.

[27] A. Genovese, R.A. Shanks, Simulation of the specific interactions between polyamide-6 and a thermoplastic polyurethane, Comput. Theor. Polym. Sci. 11 (2001) 57–62.

[28] P.D. Neis, N.F. Ferreira, J.C. Poletto, J. Sukumaran, M. Andó, Y. Zhang, Tribological behavior of polyamide-6 plastics and their potential use in industrial applications, Wear. 376 (2017) 1391–1398.

[29] M. Arhant, C. Briançon, C. Burtin, P. Davies, Carbon/polyamide 6 thermoplastic composite cylinders for deep sea applications, Compos. Struct. 212 (2019) 535–546.

[30] S.S. Kumar, G. Kanagaraj, Evaluation of mechanical properties and characterization of silicon carbide–reinforced polyamide 6 polymer composites and their engineering applications, Int. J. Polym. Anal. Charact. 21 (2016) 378–386.

[31] J. Matulevicius, L. Kliucininkas, D. Martuzevicius, E. Krugly, M. Tichonovas, J. Baltrusaitis, Design and characterization of electrospun polyamide nanofiber media for air filtration applications, J. Nanomater. 2014 (2014).

[32] H.-D. Nguyen-Tran, V.-T. Hoang, V.-T. Do, D.-M. Chun, Y.-J. Yum, Effect of

multiwalled carbon nanotubes on the mechanical properties of carbon fiber-reinforced polyamide-6/polypropylene composites for lightweight automotive parts, Materials (Basel). 11 (2018) 429.

[33] J.J. Murray, T. Allen, S. Bickerton, A. Bajpai, K. Gleich, E.D. McCarthy, C.M. Ó Brádaigh, Thermoplastic RTM: Impact Properties of Anionically Polymerised Polyamide 6 Composites for Structural Automotive Parts, Energies. 14 (2021) 5790.

[34] G. Ćwikła, C. Grabowik, K. Kalinowski, I. Paprocka, P. Ociepka, The influence of printing parameters on selected mechanical properties of FDM/FFF 3D-printed parts, in: IOP Conf. Ser. Mater. Sci. Eng., IOP Publishing, 2017: p. 12033.

[35] J. Suteja, Effect of Infill Pattern, Infill Density, and Infill Angle on the Printing Time and Filament Length of 3D Printing, Rekayasa Mesin. 12 (2021) 145–152.

[36] B. Akhoundi, A.H. Behravesh, Effect of filling pattern on the tensile and flexural mechanical properties of FDM 3D printed products, Exp. Mech. 59 (2019) 883–897.

[37] H. Vahabi, F. Laoutid, M. Mehrpouya, M.R. Saeb, P. Dubois, Flame retardant polymer materials: An update and the future for 3D printing developments, Mater. Sci. Eng. R Reports. 144 (2021) 100604.

[38] Y. Guo, C.-C. Chang, G. Halada, M.A. Cuiffo, Y. Xue, X. Zuo, S. Pack, L. Zhang, S. He, E. Weil, Engineering flame retardant biodegradable polymer nanocomposites and their application in 3D printing, Polym. Degrad. Stab. 137 (2017) 205–215.

[39] L. Geoffroy, F. Samyn, M. Jimenez, S. Bourbigot, Additive manufacturing of fire-retardant ethylene-vinyl acetate, Polym. Adv. Technol. 30 (2019) 1878–1890.

[40] M.-J. Chen, S. Lazar, T.J. Kolibaba, R. Shen, Y. Quan, Q. Wang, H.-C. Chiang, B. Palen, J.C. Grunlan, Environmentally benign and self-extinguishing multilayer nanocoating for protection of flammable foam, ACS Appl. Mater. Interfaces. 12 (2020) 49130–49137.

[41] H. Wu, A. Kafi, H. Kim, R. Shah, S. Bateman, J.H. Koo, Additive manufacturing of

flame-retardant polyamide 6 nanocomposites via fused filament fabrication (FFF), SAMPE 2019-Charlotte, NC, May 2019. (2019).

[42] E. Totry, J.M. Molina-Aldareguía, C. González, J. LLorca, Effect of fiber, matrix and interface properties on the in-plane shear deformation of carbon-fiber reinforced composites, Compos. Sci. Technol. 70 (2010) 970–980.

[43] L. Geoffroy, F. Samyn, M. Jimenez, S. Bourbigot, Innovative 3D printed design to conceive highly fire-retardant multi-material, Polym. Degrad. Stab. 169 (2019) 108992.

[44] L. Zárybnická, P. Mácová, D. Machová, J. Rychlý, A. Viani, The effect of 3D structure design on fire behavior of polyethylene terephthalate glycol containing aluminum hypophosphite and melamine cyanurate, J. Appl. Polym. Sci. 138 (2021) 50072.

[45] M.S. Saharudin, J. Hajnys, T. Kozior, D. Gogolewski, P. Zmarzły, Quality of surface texture and mechanical properties of PLA and PA-based material reinforced with carbon fibers manufactured by FDM and CFF 3D printing technologies, Polymers (Basel). 13 (2021) 1671.

[46] Y.-Y. Zhang, Z. Sun, Y.-Q. Li, P. Huang, Q. Chen, S.-Y. Fu, Tensile creep behavior of short-carbon-fiber reinforced polyetherimide composites, Compos. Part B Eng. 212 (2021) 108717.

[47] H. Wang, D.J. Kline, M.C. Rehwoldt, M.R. Zachariah, Carbon Fibers Enhance the Propagation of High Loading Nanothermites: In Situ Observation of Microscopic Combustion, ACS Appl. Mater. Interfaces. 13 (2021) 30504–30511.

[48] ISO 527-1:2019. Plastics — Determination of tensile properties — Part 1: General principles., 2019.

[49] ISO 5660-1:2015 - Reaction-to-fire tests — Heat release, smoke production and mass loss rate — Part 1: Heat release rate (cone calorimeter method) and smoke production rate (dynamic measurement), (n.d.).

[50] M. Schmid, A. Amado, K. Wegener, Polymer powders for selective laser sintering (SLS), in: AIP Conf. Proc., AIP Publishing LLC, 2015: p. 160009.

[51] J.H. Eun, D.H. Kim, J.S. Lee, Effect of low melting temperature polyamide fiber-interlaced carbon fiber braid fabric on the mechanical performance and fracture toughness of CFRP laminates, Compos. Part A Appl. Sci. Manuf. 137 (2020) 105987.

[52] C. Pascual-González, M. Iragi, A. Fernández, J.P. Fernández-Blázquez, L. Aretxabaleta, C.S. Lopes, An approach to analyse the factors behind the micromechanical response of 3D-printed composites, Compos. Part B Eng. 186 (2020) 107820.

[53] A. Kwaśniewska, D. Chocyk, G. Gładyszewski, J. Borc, M. Świetlicki, B. Gładyszewska, The influence of kaolin clay on the mechanical properties and structure of thermoplastic starch films, Polymers (Basel). 12 (2020) 73.

[54] J.M. Chacón, M.A. Caminero, P.J. Núñez, E. García-Plaza, I. García-Moreno, J.M. Reverte, Additive manufacturing of continuous fibre reinforced thermoplastic composites using fused deposition modelling: Effect of process parameters on mechanical properties, Compos. Sci. Technol. 181 (2019) 107688.

[55] F. Kaji, A. Barari, Evaluation of the surface roughness of additive manufacturing parts based on the modelling of cusp geometry, IFAC-PapersOnLine. 48 (2015) 658–663.

[56] M. Kumar, R. Ramakrishnan, A. Omarbekova, 3D printed polycarbonate reinforced acrylonitrile–butadiene–styrene composites: Composition effects on mechanical properties, micro-structure and void formation study, J. Mech. Sci. Technol. 33 (2019) 5219–5226.

[57] H. Zhang, J. Lu, H. Yang, J. Lang, H. Yang, Comparative study on the flame-retardant properties and mechanical properties of PA66 with different dicyclohexyl hypophosphite acid metal salts, Polymers (Basel). 11 (2019) 1956.

[58] F. Puch, C. Hopmann, Morphology and tensile properties of unreinforced and short

carbon fibre reinforced Nylon 6/multiwalled carbon nanotube-composites, Polymer (Guildf). 55 (2014) 3015–3025.

[59] R.A. Mensah, Q. Xu, S. Asante-Okyere, C. Jin, G. Bentum-Micah, Correlation analysis of cone calorimetry and microscale combustion calorimetry experiments, J. Therm. Anal. Calorim. 136 (2019) 589–599. https://doi.org/10.1007/s10973-018-7661-5.

[60] G.E. Zaikov, S.M. Lomakin, Ecological issue of polymer flame retardancy, J. Appl. Polym. Sci. 86 (2002) 2449–2462.

[61] R.A. Mensah, D.A. Edström, O. Lundberg, V. Shanmugam, L. Jiang, X. Qiang, M. Försth, G. Sas, M. Hedenqvist, O. Das, The effect of infill density on the fire properties of polylactic acid 3D printed parts: A short communication, Polym. Test. 111 (2022) 107594.

[62] P.R. Hornsby, Fire retardant fillers for polymers, Int. Mater. Rev. 46 (2001) 199–210.

[63] B. Schartel, T.R. Hull, Development of fire-retarded materials—Interpretation of cone calorimeter data, Fire Mater. 31 (2007) 327–354. https://doi.org/10.1002/fam.949.